Improvement of energy dissipative particle dynamics method to increase accuracy

Marzie Borhani & Somaye Yaghoubi

Journal of Thermal Analysis and Calorimetry
An International Forum for Thermal Studies

ISSN 1388-6150
Volume 144
Number 6

J Therm Anal Calorim (2021)
144:2543-2555
DOI 10.1007/s10973-020-10362-1

Springer

Journal of Thermal Analysis and Calorimetry (2021) 144:2543–2555
https://doi.org/10.1007/s10973-020-10362-1

Improvement of energy dissipative particle dynamics method to increase accuracy

Marzie Borhani[1] · **Somaye Yaghoubi**[1]

Received: 23 June 2020 / Accepted: 13 October 2020 / Published online: 19 November 2020

Abstract
In this article, dissipative particle dynamics with energy conservation eDPD is used for simulating hydrodynamic behavior and heat transfer of DPD particles in a two-dimensional channel with parallel planes. To this end, a Fortran programming code is developed and the results are presented as dimensionless velocity and temperature profiles on the cross section perpendicular to the flow direction inside the channel. For the indented geometry, thermal and dynamic boundary conditions have been considered. The dynamic boundary condition of solution domain in the flow's direction is periodic, and for modeling the walls, freezing layers of DPD particles with Bounce-Back reflection has been used. For the thermal boundary condition, it is assumed that the wall temperature is constant and the temperature of each DPD particle in contact with the wall is the same as the wall temperature. In this article, for the first time, for modeling the walls four frozen layers with Bounce-Back reflection are used and the effect of particle exit on two and three-layers configurations is investigated. Furthermore, for the first time, modified velocity Verlet integration algorithm is improved by adding heat transfer equations. And considering $\lambda = 0.65$ in the algorithm; the indented geometry is well simulated. In order to validate the results, first, the effect of regular and random initial distribution is compared. Furthermore, the results of wall alignment are compared with those obtained from CFD approach. In this paper, in addition to studying the effect of wall alignment and initial particle arrangement, the influence of the size of cells for averaging and the time steps in the output results are investigated.

Keywords Dissipative particle dynamics · Heat transfer · Boundary conditions · No-slip · Meso-scale

Introduction

Various attempts have been made for the solution of fluid dynamics and heat transfer problems using methods such as computational fluid dynamics (CFD) and atomic techniques such as molecular dynamics (MD). Study and simulation of geometries in meso-scale has always been one of the favorite issues of researchers. Currently, several approaches are used in meso-scale, the most popular of which include Brownian dynamics (BD), Lattice Boltzmann method (LBM), dissipative particle dynamics (DPD) and molecular dynamics (MD). For example, molecular dynamics (MD) approach and Lattice Boltzmann method (LBM) have been used for simulating of nanofluids [1–3], slip flows [3, 4], nanotubes and microchannel [5–8], porous media [9, 10]; for example, Karimipour et.al. studied the electric field and microchannel type effects on H2O/Fe3O4 nanofluid dynamical manner using molecular dynamics [11]. Or they develop MD Method to Simulate the flow and thermal domains of H2O/Cu nanofluid in a nanochannel affected [12]. However, these approaches are not suitable for studying of mesostructured in some problems. As a result, dissipative particle dynamics (DPD) was first introduced as a particle-based approach by Hoogerbrugge and Koelman for solving hydrodynamic problems [13]. This method is very similar to the MD approach with some differences. MD method sometimes added a large number of unnecessary details to the solution [13, 14]. The equilibrium conditions in the fluctuation–dissipation theory were proposed by Español, and Warren in 1995 and 1997 and added to the DPD equations [15, 16]. In the recent decades, DPD methods have been used for various applications such as hydrodynamic simulation of particles suspended in a liquid [17–19], multiphase flow [20–22], polymers [23–26], droplets [27–29] and biological systems [30, 31], flow around spheres and cylinders [32–35], microchannels,

✉ Somaye Yaghoubi
s.yaghoubi@pmc.iaun.ac.ir

[1] Department of Mechanical Engineering, Najafabad Branch, Islamic Azad University, Najafabad, Iran

nanochannels and nanoparticles [36–39]. For example, Yaghoubi, et.al. introduced a new weight function in this method and used it to simulate flows with values close to the real Schmitt number [40]. In another study, they showed that using DPD particles with intrinsic size can help reduce the number of particles required for the simulation. This decrease in the number of particles in turn results in a more feasible simulation [41]. The energy conservation model for simulation of one-dimensional conduction heat transfer was introduced by Ripoll et.al. and Ripoll and Español in 1998 and 2000. Along with satisfying the Fourier law, this model also correctly depicted the equilibrium variations [42]. Dissipative particle dynamics method with energy conservation is known as eDPD. Qiao and He [35] used eDPD for thermal conductivity of nanocomposites and heat transfer in nanofluids [43, 44]. Borhani and Yaghoubi investigated the behaviors of different weight functions on the wall of a two-dimensional channel and presented the results as dimensionless velocity and temperature profiles. They showed that weight function with higher dissipative viscosity is more suitable for accurate estimation of wall characteristics and the profiles [45]. Abu-dana, used eDPD in order to apply various thermal boundary conditions in 2D heat transfer problems. These boundaries included constant temperature, constant heat flux and adiabatic conditions [46]. He also simulated 2D thermal conductivity in another study and correctly modeled Derlikke and Neumann boundary conditions and compared them with the analytical results [47]. In 1999, Mackie et.al. used eDPD for two conduction and convection heat transfer scenarios [48]. Yamada et.al. used eDPD for modeling of forced convection for constant temperature and constant heat flux boundary conditions. They then calculated the Nusselt number for both conditions and compared the results with the analytical solution. The error was estimated to be 2.3% compared with the analytical solution [49].

One of the most important problem in this method is wall modeling and the effect of fluid particles entering the wall layers; therefore, due to the importance of the particle behavior near the wall, for the first time, in the current study four frozen layers are used along with Bounce-Back reflection and the effect of particle output on two and three-layers configurations is investigated. In addition, integration algorithms have been used to solve the conservation equations and determining the location, velocity and temperature of each DPD particle. Also these integration algorithms have been used to determine the force and net heat flux. Furthermore, in this study, for the first time, modified velocity Verlet integration algorithm was improved by adding heat transfer equations with relaxation factor of $\lambda = 0.65$. In order to validate the created code, it is investigated whether initial DPD particles distribution affect the behavior of the particles and final results in equilibrium. Also, the results were compared with those obtained from CFD approach.

In this article, "Theory" section presents the equations in DPD approach before explaining the hydrodynamic and thermal boundary conditions of the problem. Then, the integration and search algorithms used in this study are introduced. In the next section, the simulated results are presented, but at first, the effect of initial regular and random configuration on the equilibrium is investigated. Then, the effect of particle's exits in dimensionless temperature and velocity profiles in two and three-layers configurations on the walls are presented and compare with CFD approach for validation. Also, the relative error values are reported. Finally, the effect of cell size in the averaging on the solution domain and time steps in the output results is investigated. The "Results and discussion" section presents a final conclusion based on the results and discussions.

Theory

Governing equations

This section first introduces equations governing DPD before expanding these equations by assigning a temperature to each particle and presenting conservation (mass, momentum and energy) equations. The forces in DPD approach can be divided into three categories of conservative forces $\vec{F}_{ij}^{C}$; Dissipative forces $\vec{F}_{ij}^{D}$; and random forces $\vec{F}_{ij}^{R}$. These forces transfer between in pairs for each two particles interacting with each other. The DPD forces have a short natural range. This means that each particle can only interact with its neighboring particles. This neighborhood is determined using a distance called cutoff radius or r_c [49]:

$$\vec{F}_{ij}^{C} = F_{ij}^{C}(r_{ij})\vec{e}_{ij} \tag{1}$$

$$\vec{F}_{ij}^{D} = -\gamma_{ij} w^{D}(r_{ij})(\vec{e}_{ij} \cdot \vec{v}_{ij})\vec{e}_{ij} \tag{2}$$

$$\vec{F}_{ij}^{R} = \sigma_{ij} w^{R}(r_{ij})\xi_{ij}\Delta t^{-1/2}\vec{e}_{ij} \tag{3}$$

In which $\vec{e}_{ij} = \vec{r}_{ij}/r_{ij}$ is the unit vector in the direction of the line connecting particles i and j. Furthermore, $\vec{r}_{ij} = \vec{r}_i - \vec{r}_j$ and r_{ij} is the length of vector $\vec{r}_{ij}$. F_{ij}^{C} is defined as weight function of conservative force; $w^{D}(r_{ij})$ and $w^{R}(r_{ij})$ are dissipative and random weight functions, respectively, and γ_{ij} and σ_{ij} are the domain of dissipative and random forces, respectively.

The dissipative force F^{D} is added for decrease in relative velocity between DPD particles. This force simulates the effects of viscosity in the system and is a function of relative velocity and distance between particles. The random or fluctuating force, F^{R}, is added to the system for creating the necessary degrees of freedom. In fact, when large granulation

technique is used, the real degrees of freedom in the system decrease. As a result of decrease in degrees of freedom, Brownian motion is not observed in the particles. In order to compensate this effect, it is necessary to add a term for interaction forces. This force is the term which results in increase in system temperature with increase in particles' movement.

Based on fluctuation–dissipation theory, random and dissipative weight functions follow Eq. 4. Furthermore, the domain of random and dissipative forces is defined according to Eq. 5 [50]:

$$\omega^{\mathrm{D}}(r) = \left(\omega^{\mathrm{R}}(r)\right)^2 \tag{4}$$

$$\gamma = \frac{\sigma^2}{2k_{\mathrm{B}}T} \tag{5}$$

Equation 4 is used in classic DPD, and Eq. 5 presents the necessary condition for equilibrium between random and dissipative forces in order to reach an isothermal system. In the eDPD approach, each DPD particle is assigned a temperature along with a velocity value and DPD equations are revised.

$$C_{\mathrm{v}}\frac{\mathrm{d}T_{\mathrm{i}}}{\mathrm{d}t} = q_{\mathrm{i}} \tag{9}$$

In which, q_{i} is the heat flux between particle and C_{v} is the heat capacity of DPD particles at constant volume. Usually, the heat capacity of DPD particles is used in its dimensionless format or $\overline{C}_v = {C_v}/{k_B}$, where k_{B} is the Boltzmann constant. Therefore, heat flux q_{i} is defined as follows [49]:

$$q_{\mathrm{i}} = \sum_{\substack{i\neq j\\ j=1}}^{N} q_{\mathrm{ij}} = \sum_{\substack{i\neq j\\ j=1}}^{N}\left(q_{\mathrm{ij}}^{\mathrm{visc}} + q_{\mathrm{ij}}^{\mathrm{cond}} + q_{\mathrm{ij}}^{\mathrm{R}}\right) \tag{10}$$

In which the first term shows the viscose heat flux, the second term shows the convection heat flux and the last term belongs to random heat flux. It is worth mentioning that the sums used in conservation laws should be applied on particles located inside the cutoff radius r_{C}. Replacing these heat flux equations results in the following energy conservation equation:

$$q_{\mathrm{i}} = \sum_{\substack{i\neq j\\ j=1}}^{N}\left[\left(\frac{1}{2C_{\mathrm{v}}}\left(w^{\mathrm{D}}(r_{\mathrm{ij}})\left[\gamma_{\mathrm{ij}}\left(\vec{e}_{\mathrm{ij}}\cdot\vec{v}_{\mathrm{ij}}\right)^2 - \frac{\sigma_{\mathrm{ij}}^2}{m_{\mathrm{i}}}\right] - \sigma_{\mathrm{ij}}w^{\mathrm{R}}(r_{\mathrm{ij}})\left(\vec{e}_{\mathrm{ij}}\cdot\vec{v}_{\mathrm{ij}}\right)\xi_{\mathrm{ij}}\right)\right) + \left(\kappa_{\mathrm{ij}}w^{\mathrm{R2}}(r_{\mathrm{ij}})\left(\frac{1}{T_{\mathrm{i}}} - \frac{1}{T_{\mathrm{j}}}\right)\right) + \left(\alpha_{\mathrm{ij}}w^{\mathrm{R}}(r_{\mathrm{ij}})\Delta t^{-\frac{1}{2}}\xi_{\mathrm{ij}}^{\mathrm{e}}\right)\right] \tag{11}$$

In the eDPD approach, conservation laws govern particles' movements. The movement equation for ith particle is defined as follows [49]:

$$\frac{\mathrm{d}\vec{r}_{\mathrm{i}}}{\mathrm{d}t} = \vec{v}_{\mathrm{i}} \tag{6}$$

$$m_{\mathrm{i}}\frac{\mathrm{d}\vec{v}_{\mathrm{i}}}{\mathrm{d}t} = \vec{f}_{\mathrm{i}} = \vec{f}_{\mathrm{i}}^{\mathrm{int}} + \vec{f}_{\mathrm{i}}^{\mathrm{ext}} \tag{7}$$

where $\vec{r}_{\mathrm{i}}$ and $\vec{v}_{\mathrm{i}}$ are the location and velocity of the ith particle; m_{i} is the mass of that and $\vec{f}_{\mathrm{i}}^{\mathrm{ext}}$ is the applied external forces such as gravity, while $\vec{f}_{\mathrm{i}}^{\mathrm{int}}$ is defined based on Eq. 8 [49]:

$$\vec{f}_{\mathrm{i}}^{\mathrm{int}} = \sum_{\substack{i\neq j\\ j=1}}^{N}\vec{F}_{\mathrm{ij}} = \sum_{\substack{i\neq j\\ j=1}}^{N}\left(\vec{F}_{\mathrm{ij}}^{\mathrm{C}} + \vec{F}_{\mathrm{ij}}^{\mathrm{D}} + \vec{F}_{\mathrm{ij}}^{\mathrm{R}}\right) \tag{8}$$

In this equation, N is the total number of particles, $\vec{F}_{\mathrm{ij}}$ is the force applied to particle i by particle j, so that $\vec{F}_{\mathrm{ij}} = \vec{F}_{\mathrm{ji}}$ because all forces in this approach have the dual action–reaction nature. Therefore, the conservation of linear momentum is maintained. On the other hand, due to constant number of particles in the system during simulation, the conservation of mass is satisfied. In the eDPD approach, due to assignment of temperature T_{i} to particle i, it is necessary to satisfy energy conservation law. This can be written as Eq. 9 [49]:

In which, κ_{ij} and α_{ij} are the powers of convection and random heat fluxes, T_{i} and T_{j} are the temperature of particle i and j, respectively, and Δt is the time step. Furthermore, $\xi_{\mathrm{ij}}^{\mathrm{e}}$ is a random number with mean of zero and variance of 1. Each pair of particles in the equilibrium results in a $\xi_{\mathrm{ij}}^{\mathrm{e}}$ value so that $\xi_{\mathrm{ij}}^{\mathrm{e}} = -\xi_{\mathrm{ji}}^{\mathrm{e}}$. The negative sign is placed in order to satisfy energy conservation equations.

In the eDPD approach, due to addition of temperature to the particles, it is necessary to use particles' temperature instead of the T in Eq. 5. In fact, T in Eq. 5 is the harmonic average of the temperature of i and j particles.

$$T = \frac{2T_{\mathrm{i}}T_{\mathrm{j}}}{T_{\mathrm{i}} + T_{\mathrm{j}}} \tag{12}$$

By replacing Eq. 12 in 5, the modified random dissipative equation for eDPD systems is created:

$$\gamma = \frac{\sigma^2\left(T_{\mathrm{i}} + T_{\mathrm{j}}\right)}{4k_{\mathrm{B}}T_{\mathrm{i}}T_{\mathrm{j}}} \tag{13}$$

where κ_{ij} and α_{ij} are the convection and random heat fluxes similar to Eq. 11 and defined as follows [49]:

$$\kappa_{\mathrm{ij}} = \frac{C_{\mathrm{v}}^2 k_0\left(T_{\mathrm{i}} + T_{\mathrm{j}}\right)^2}{4k_{\mathrm{B}}} \tag{14}$$

$$\alpha_{ij} = \sqrt{2k_B\kappa_{ij}} \tag{15}$$

In this equation, k_B is the Boltzmann constant and k_0 is a control parameter of thermal conductivity of eDPD particles. The value of k_0 is empirical and is determined by comparing the results of this solution with the finite volume method for the same geometry.

Furthermore, in this article, the classic weight function [51] is used:

$$\omega^D(r) = \left(\omega^R(r)\right)^2 = \begin{cases} 1 - \frac{r_{ij}}{r_C} & r_{ij} \le r_C \\ 0 & r_{ij} > r_C \end{cases} \tag{16}$$

Integration algorithms

Abu-dana [52] in 2014 expanded the Grout–Warren algorithm by adding energy conservation equations. According to this algorithm, the V-V used in eDPD approach is as follows:

Step 1:

$$r_i(t+\Delta t) = r_i(t) + \Delta t v_i(t) + \frac{1}{2}(\Delta t)^2 f_i(t)$$

Step 2:

$$\widetilde{v}_i(t+\Delta t) = v_i(t) + \lambda \Delta t f_i(t)$$

$$\widetilde{T}_i(t+\Delta t) = T_i(t) + \frac{\lambda}{C_v}\Delta t f_i(t)$$

Step 3:

$$f_i(t+\Delta t) = f_i\left(r_i(t+\Delta t), \widetilde{v}_i(t+\Delta t)\right)$$

$$q_i(t+\Delta t) = q_i\left(r_i(t+\Delta t), \widetilde{v}_i(t+\Delta t), \widetilde{T}_i(t+\Delta t)\right)$$

Step 4:

$$v_i(t+\Delta t) = v_i(t) + \frac{1}{2}\Delta t\left(f_i(t) + f_i(t+\Delta t)\right)$$

$$T_i(t+\Delta t) = T_i(t) + \frac{1}{2C_v}\Delta t\left(q_i(t) + q_i(t+\Delta t)\right) \tag{17}$$

In the second step, along with estimated velocity, an estimated temperature is also assigned to the particles which is the result of temperature and heat flux calculated in the previous time step. In the third step, after updating the forces, the heat flux is also updated. The important part is the presence of estimated velocity $\widetilde{v}_i(t+\Delta t)$ which is required in the viscose heat flux. In the final step, along with modifying the velocity, particles' temperatures are also updated. In the current article, for the first time a combination of this algorithm with modified velocity Verlet is used for modeling heat transfer using DPD approach with relaxation factor of $\lambda = 0.65$. Choosing a larger value for λ means that the time steps can be larger. However, this value should be optimized because a very large relaxation factor results in high integration error. Although this algorithm does not satisfy time reversibility condition, but it is an accurate method for integration of conservation equations and has a reasonable calculation cost [53].

Boundary conditions

The current study uses particle freezing and Bounce-Back reflection approach together for modeling of channel walls. In this reflection, it is assumed that after impacting the wall, the particles return to the fluid in the opposite direction of their initial path. This means that tangent and normal components of the momentum are inversed.

$$\left(V_n\right)_{\text{After Collision}} = -V_n \tag{18}$$

$$\left(V_t\right)_{\text{After Collision}} = -V_t$$

In order to simulate constant temperature boundary condition, it is assumed that each particle with an initial temperature (different or equal to the wall temperature) adsorbs heat from the wall after impacting the wall with constant temperature and returns to the fluid.

The dimensionless temperature for temperature boundary condition on the wall is showed as follows:

$$\theta = \frac{T - T_w}{T_m - T_w} \tag{19}$$

In which, T_w is the wall temperature, T is the local fluid temperature and T_m is the mean temperature in the fluid cross section. It is worth noting that the dimensionless temperature gradient is not dependent on x, therefore, thermal expansion condition of this parameter is shown as $\frac{\partial\theta}{\partial x} = 0$.

The mean temperature is calculated using the following equation:

$$T_m - T_w = \frac{\int_{Ac}\left(T - T_w\right)u\mathrm{d}z}{\int_{Ac} u\mathrm{d}z} \tag{20}$$

In some cases, it is necessary to calculate fluid properties in infinite domains. Using periodic boundary condition, the calculation domain will gain a periodic nature and the repeat of the images in this domain continues to infinity. The mechanism of this boundary means that around the solution domain, images of the solution are created in various directions and these images fill the entire calculation space.

This is despite the fact that the problem is only solved for that range and its answers are generalized to infinity. The periodic boundary condition is a general condition: in the current article, since in the channel, z direction is perpendicular to the flow direction, periodic boundary condition is applied in the x direction. Therefore, particles exit the solution domain and reenter the domain with similar velocity and position. For the isotherm temperature boundary condition, the dimensionless temperature should be determined using the following equation [49]:

$$(x, z) = \theta(x + l, z) = \theta(x + 2l, z) = \ldots \tag{21}$$

Therefore, temperature field in the fully developed region repeats at certain time intervals. The differentiating the dimensionless temperature difference versus the time results in the following equation:

$$\frac{\mathrm{d}\theta}{\mathrm{d}t} = \frac{1}{T_\mathrm{m} - T_\mathrm{w}} \frac{\mathrm{d}T}{\mathrm{d}t} + \frac{T - T_\mathrm{w}}{\left(T_\mathrm{m} - T_\mathrm{w}\right)^2} \frac{\mathrm{d}T_\mathrm{m}}{\mathrm{d}t} \tag{22}$$

In the fully developed flow regime, $\frac{\mathrm{d}T_\mathrm{m}}{\mathrm{d}t} = 0$ and therefore:

$$\frac{\mathrm{d}T}{\mathrm{d}t} = \left(T_\mathrm{m} - T_\mathrm{w}\right) \frac{\mathrm{d}\theta}{\mathrm{d}t} \tag{23}$$

By combining Eqs. (23) and (7), the modified equation for constant temperature condition of the wall is as follows [49]:

$$\frac{\mathrm{d}\theta}{\mathrm{d}t} = \frac{1}{C_\mathrm{v}\left(T_\mathrm{m} - T_\mathrm{w}\right)} \left(q_\mathrm{ij}^\mathrm{visc} + q_\mathrm{ij}^\mathrm{cond} + q_\mathrm{ij}^\mathrm{R}\right) \tag{24}$$

Search Algorithms

Since forces and heat fluxes have short-range nature in eDPD, it is possible to significantly reduce the calculation volume necessary for searching for particles. Therefore, in order to improve the calculations, it is necessary to present a rapid solution. The general idea behind search algorithms is that in order to calculate the force and heat flux of a particle, it is sufficient to investigate its neighboring particles in a cutoff radius r_C in each step. This means that in search algorithms, the goal is finding particles present in this neighborhood. In this article, a cellular search algorithm is used. In this algorithm, the domain is divided into $M \times M \times M$ cells. The dimension of each cell in this network is defined as $l = L/M$ and should be determined so that it is slightly larger than the cutoff radius. Therefore, it can be said that particles in each cell can only interact with the particles in the same cell and its neighboring cells and it is not necessary to investigate other cells. This results in a significant reduction in calculation volume. In fact, in each search, it is only necessary to calculate the cells on the right and top and add them to the reaction values previously measured for cells on the left and bottom.

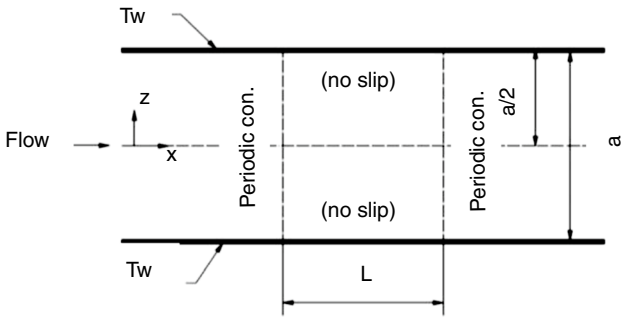

Fig. 1 The schematic of the investigate geometry

Table 1 eDPD parameters

ρ	a_ij	γ_ij	r_C	$\overline{C}_V$	k_0
4	18.75	4.5	1.0	1.0×10^5	1.26×10^{-4}

Forced Convection Heat Transfer Problems

Figure 1 shows a schematic of laminar flow in this channel. As can be seen, the flow enters the channel with the force of $F_\mathrm{ext} = 0.01$ which satisfies all constant temperature conditions in the walls. The channel's dimensions in the x and z directions are L = 5 and a = 40 and the walls have no-slip condition. Furthermore, the flow has fully developed conditions. The temperature condition on the wall is constant temperature in which the temperature values of upper and lower walls are equal to each other and $Tw = 1.$ in DPD unit. The temperature of input fluid is equal to 1.0 in DPD unit.

The constant parameters used in eDPD solution are presented in Table 1 [49]:

Results and discussion

Investigating regular and random configurations

In order to ensure the correctitude of the computer coding, regular and random configurations were investigated in the first step. In ordered configuration, fluid particles are placed in ordered layers in the channel at the beginning of the simulation. These particles have the temperature of 1.0 in DPD unit and random velocities with Gaussian distribution.

In the random configuration, particles are placed randomly at the initial time. For the velocity and temperature, the values are the same as in ordered case. These two configurations at the initial time are shown in Fig. 2.

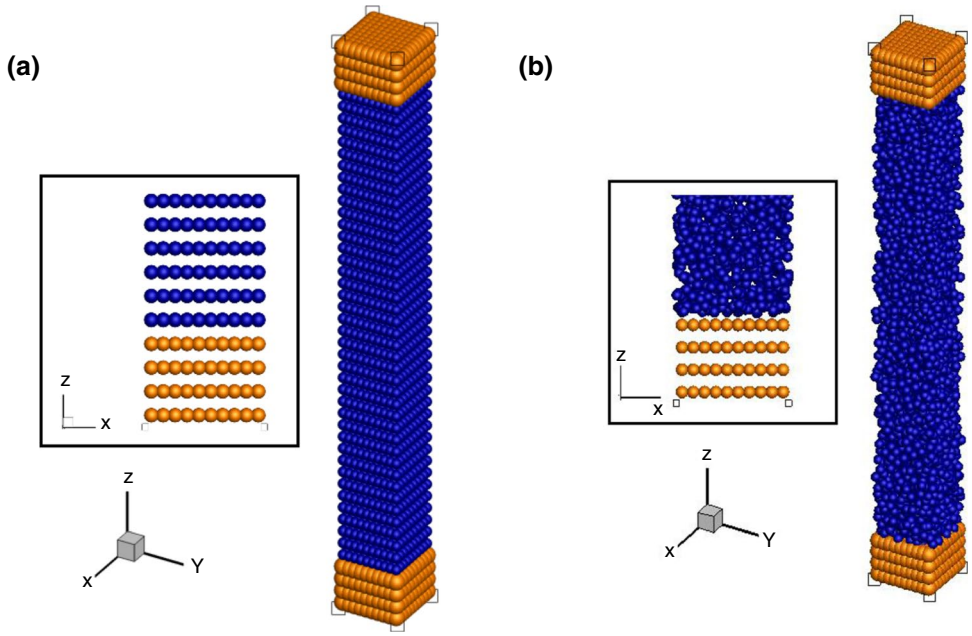

Fig. 2 **a** Ordered and **b.** random configuration of eDPD particle

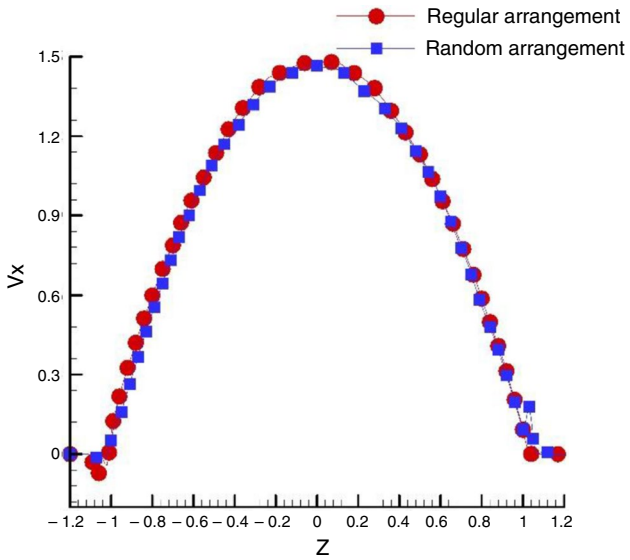

Fig. 3 Effect of initial configuration on dimensionless velocity profile in equilibrium

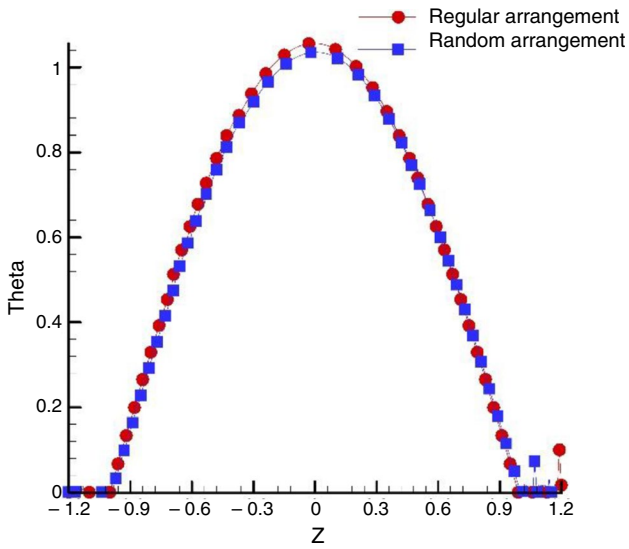

Fig. 4 Effect of initial configuration on dimensionless temperature profile in equilibrium

Figures 3 and 4 show the velocity and the dimensionless temperature difference profile for regular and random initial distribution. As can be seen, the initial configuration has no effects on velocity and temperature profiles in equilibrium. In fact, due to the presence of interacting forces and heat flux between eDPD particles in the initial time step, ordered configuration is destroyed and eDPD particles move to the positions determined through movement equations.

The number of frozen layers required for wall modeling

In this section, the effect of number of frozen layers on the wall modeling is investigated. In order to prevent the particles from escaping the solution domain, wall particle freezing is used. This adds the wall's characteristics to the calculation domain while also acting as a barrier preventing the exiting of fluid particles. Furthermore, the density of the wall and fluid is a constant number presented in Table 1. The reason for using equal density in these two environments is

to prevent density variations near the wall. When the fluid particles reach wall particles in their cutoff radius, they will be affected by an imaginary gravitational force in case of difference in density which results in increased error. In previous studies [54–56], two frozen layers are used to this end. Using the same approach, the geometry investigated in the current study also initially used two frozen layers as the wall. However, after reaching the steady state and evaluating the velocity profiles, unacceptable variations were observed near the wall. A more careful investigation of the wall showed that fluid particles have exited the channel as shown in Fig. 5. The three-layer configuration is also shown in this fig.

The velocity profiles for two and three-layers configuration wall are presented in Fig. 6. As can be seen, in the fluid area and specially in the estimation of maximum velocity at the center of the channel, both configurations show acceptable compatibility with CFD solution results. The estimated maximum velocity in two and three-layer configurations was equal to $V_{2L} = 1.480$ and $V_{3L} = 1.491$, which, when compared to the CFD value of $V_{CFD} = 1.50$, show 1.3% and 0.6% error, respectively. However, close to the wall, due to the diffusion of fluid particles into the solid area, a large amount of variation is observed. These variations are not dependent on the number of diffused particles and instead depend on the velocity of these particles. These variations have resulted in an error of 40% for two-layer configuration and an error of 14.6% for the three-layer configuration in the dimensionless velocity profile.

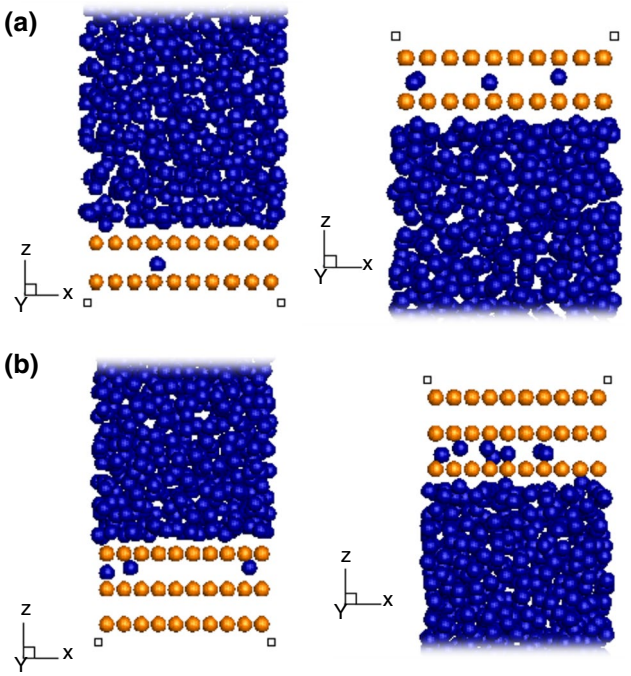

Fig. 5 Particles exiting through the wall in **a.** two-layer configuration **b.** three-layer configuration

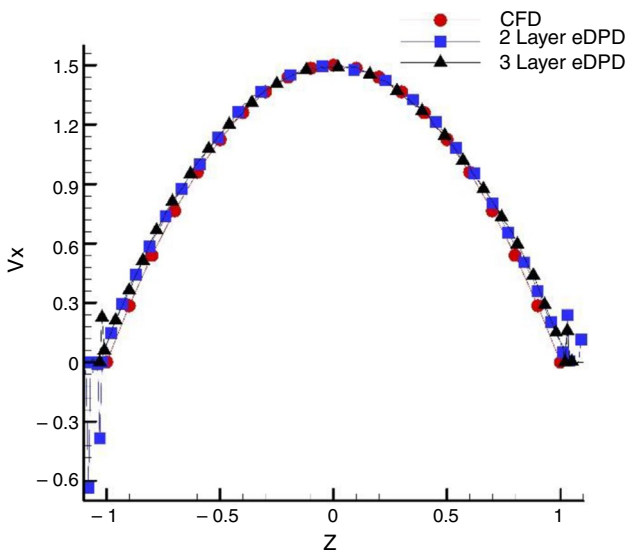

Fig. 6 The velocity profile in different wall configurations

The dimensionless temperature difference profiles for different number of frozen layers are shown in Fig. 7. As can be seen, diffusion of particles in the wall has resulted in significant variations in the temperature profile. These variations are higher in two-layer configuration such that this configuration has an error of 33.7% on the upper wall.

Based on the observations in this section, a four-layer wall configuration was used which presents in more accurate results compared to two and three-layer configurations has smaller amount of particle diffusion. The result of this simulation is presented in the following sections.

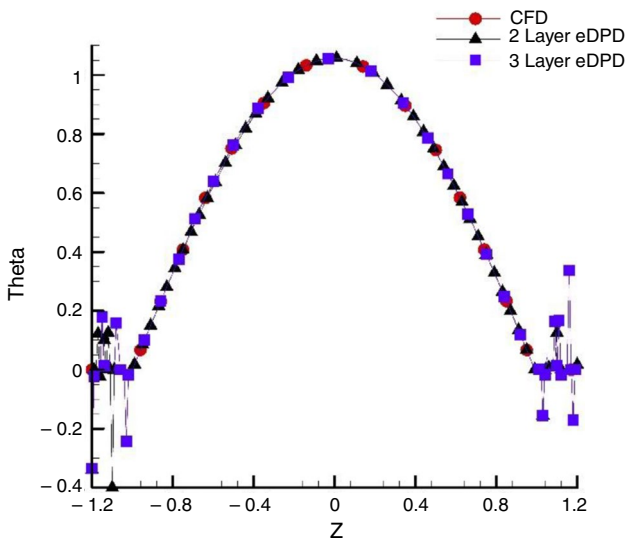

Fig. 7 The dimensionless temperature difference profile at different wall configurations

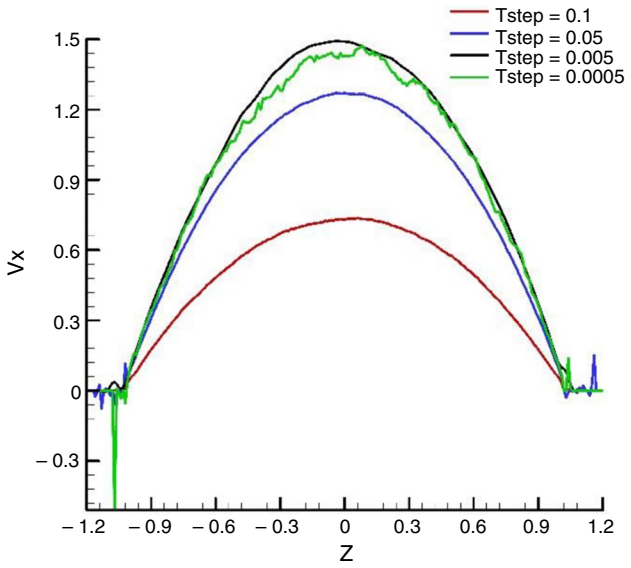

Fig. 8 The effect of time step on the velocity profile

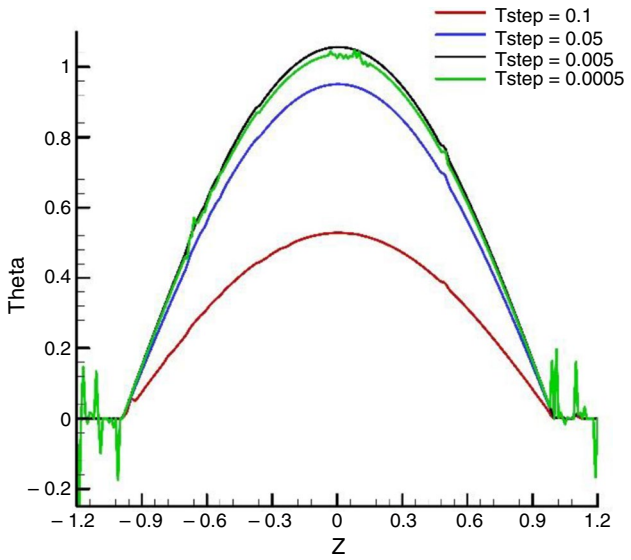

Fig. 9 The effect of time step on dimensionless temperature difference profile (constant wall temperature)c

Effect of time step

One of the most important factors in numerical calculations is the selection of proper time steps. Time steps should be selected in a way that maintain the details of the calculations while preventing unfeasibly large calculation costs. A large time step results in rounding error, while small time steps increase the number of repeated calculations and therefore the time necessary for reaching steady state. In the current study, the effect of time steps on output results was investigated. To this end, four different time steps of dt = 0.1; 0.05; 0.005 and 0.0005 s were selected.

Figures 8 and 9 show the velocity and temperature profiles. At dt = 0.1 s; due to the large time step, a large number of particles have diffused through the wall and the problem has failed to correctly simulate the interactions between the fluid and the walls. This system is also unable to estimate mean velocity and maximum velocity profiles which has resulted in divergence of the problem. In the time step of dt = 0.05 s, similar to the previous time step, a large number of particles have diffused through the wall and the velocity profile still shows a significant difference with CFD results. The maximum velocity in this case as an error of 20% compared to CFD results and in the dimensionless temperature graph for constant temperature boundary condition, a constant error of 9.5% is observed. Therefore, it is necessary to reduce the time step. At dt = 0.005 s, the highest errors in velocity profile near the wall and at the center of channel are 2.8% and 0.66%, respectively, while dimensionless temperature profile has an error of 1.1% and 0.31% at these two positions. Now, it is necessary to determine whether further decrease in time step can lead to significant improvement in the results.

At dt = 0.0005 s, the velocity and temperature profiles are almost identical to the results obtained at dt = 0.005 s, while the variations near the walls are more severe. This is due to the increase in discretization errors which is one of the disadvantages of this time step along with increased calculation cost. Furthermore, no significant improvement in the results is observed compared to the time step of dt = 0.005 s, while the calculation cost in dt = 0.0005 is ten times higher than the calculation cost at dt = 0.005. This can be a significant disadvantage in large systems with a large number of particles. Based on these results, the optimum time step for this study was selected to be dt = 0.005 s.

Effect of number of cells in the vertical direction of the channel

In the eDPD approach, statistical averaging is used for the output results. To this end, the solution domain is divided into cells in the desired direction and the hydrodynamic and thermal properties are investigated separately in each cell. Each rectangular division is known as a single cell, and its side is called rbin. Each cell has an average velocity and temperature which are the average of the velocity and temperature for all the particles in that cell. Therefore, the number of cells can be an important parameter for increasing the accuracy of the calculations.

Due to the statistical nature of the eDPD method, the selection of rbin can greatly affect the final answers and their accuracy, which is evident in Figs. 10 and 11. The number of particles in a small rbin is low and during an averaging, one

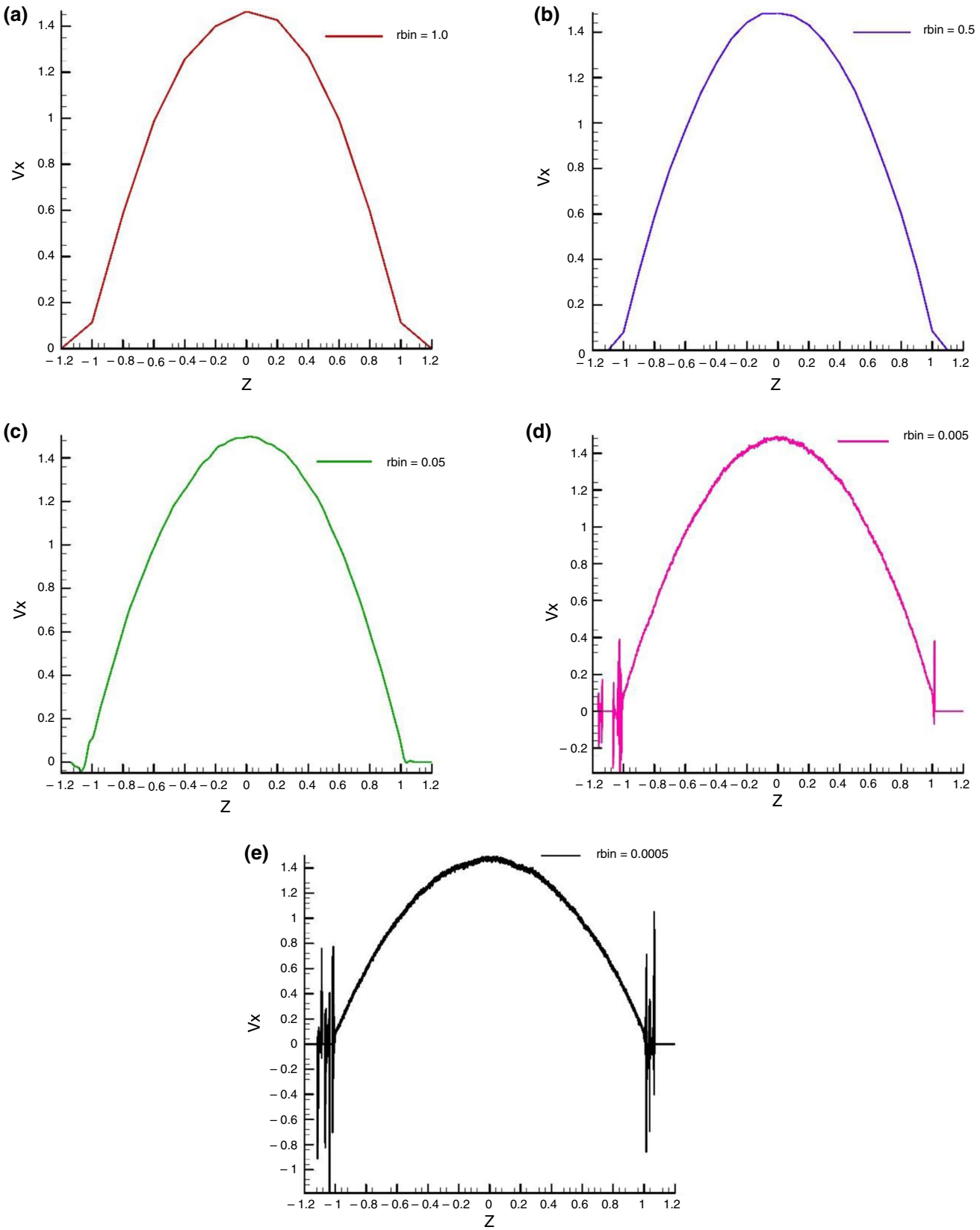

Fig. 10 The effect of averaging cell size in the z-axis direction on velocity profile **a.** rbin = 1.0, **b.** rbin = 0.5, **c.** rbin = 0.05, **d.** rbin = 0.005 and **e.** rbin = 0.005

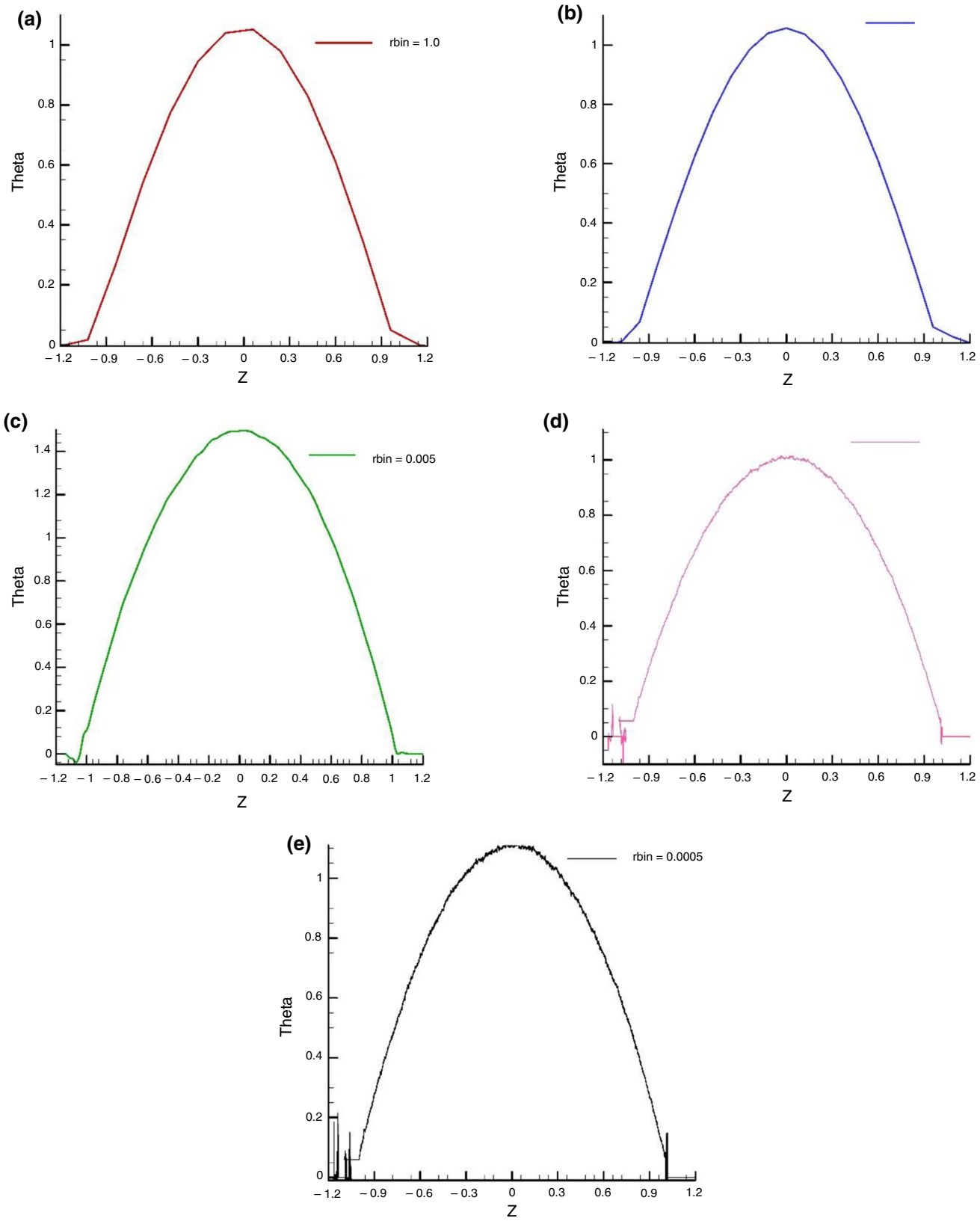

Fig. 11 The effect of averaging cell size in the z-axis direction on dimensionless temperature profile **a.** rbin = 1.0, **b.** rbin = 0.5, **c.** rbin = 0.05, **d.** rbin = 0.005 and **e.** rbin = 0.005

or two particles may be removed from the cell which has a great effect on statistical calculations and then the averaging operation may encounter an error. It is even possible to find a cell that does not contain any particles. In addition, in small rbin, due to the expensive calculations, achieving equilibrium is time consuming. In large rbin, the results are not accurate enough due to the large number of particles in each cell. Then, it is important to find an optimal size for the rbins.

Figures 10 and 11 show the effect of the number of cells in the direction of z-axis for velocity profile and dimensionless temperature profile. As can be seen, for rbin = 1.0, the velocity profile has a correct shape but is jagged. Furthermore, this profile fails to present sufficient details near the wall. For better understanding of this fact, consider a cell near the wall. Due to the large size of the cell, a large number of wall particles are placed in a single cell and their zero velocity significantly affects the average fluid velocity in that cell. Since all particles, including wall and fluid particles, in a single cell are recognized by their average velocity, this means that not only the average velocity is lower than the actual value but that an average velocity is also assigned to the wall particles, both of which result in error close to the wall. This problem is also observed in the dimensionless temperature profiles. In the velocity graph, the maximum velocity at the center of channel is estimated to be 1.46 which has 2.7% error compared to CFD results. This error has been somewhat fixed for rbin = 0.5, resulting in an error of 1.3%. However, the problem close to the wall is still observed in this case, resulting in a calculated velocity of 0.1 for wall particles. Similar to the velocity, temperature graphs also have a jagged look, while both graphs estimate correct maximum values.

For rbin = 0.05, the velocity profile has an error of less than 0.05% at its maximum, while the velocity close to the walls is also correctly predicted. Smaller rbin values result in smaller errors but reducing the cell size to rbin = 0.005 and rbin = 0.0005 results in variations in the graph. This is due to the fact that the statistical calculation used results in a set amount of error for each cell. If the number of cells exceeds an optimum amount, this error increases and results in variation in graphs and undesirable results. Furthermore, the size of cells should be selected in a way that at least one eDPD particle is present in each cell. If the cells are smaller than a certain amount, it will be possible for cells with no particles to exist, resulting in zero velocity and temperature values and calculation error.

Conclusions

In this paper, a two-dimensional channel with parallel planes was investigated using the EDPD method. By considering a temperature for each DPD particle, the heat flux term of energy conservation equations was correctly simulated. For this goal, a Fortran programming code was developed. Also, for the first time in this method, modified velocity Verlet integration algorithm was improved by adding heat transfer equations with relaxation factor of $\lambda = 0.65$. In order to properly simulate the wall configurations and preventing the exit of fluid particles from the solution domain and implementation of no-slip conditions on the walls, for the first time a four-layer frozen particle configuration and bounce-back reflection rules were employed. Also two approaches were considered to validate the written code: first, the effect of regular and random configurations was investigated in the first step and the results indicated that the type of configuration has no effects on the stability and the output results. Second, the results of this method in two and three-layer wall arrangement were compared with the results of CFD approach, which had an acceptable consistency in estimating the maximum values in the dimensionless velocity and temperature profiles. In the next step, the effect of time steps on the output results and stability was investigated. The size of time step had a direct effect on the output results, with particles diffusing into the wall at large time steps resulting in divergent solution, while small time steps resulted in variations in the velocity and temperature profile graphs due to the increase in calculation error. Therefore, the optimum time step of dt = 0.005 s was selected. Finally, the effect of averaging cell sizes in the x-axis direction of the channel was investigated. If the number of averaging cells was smaller than a certain value, details of the solution were lost. Significant increase in the number of averaging cells resulted in variations in the entire graphs which were more significant near the walls. Based on these results, the width of averaging cell was set to rbin = 0.05.

References

1. Karimipour A, Hemmat Esfe M, Safaei R, Toghraie Semiromi D, Jafari S, Kazi SN. Mixed convection of copper–water nanofluid in a shallow inclined lid driven cavity using the lattice Boltzmann method. Phys A. 2014;402:150–68. https://doi.org/10.1016/j.physa.2014.01.057.
2. Moshfegh A, Abouei Mehrizi A, Javadzadegan A, Joshaghani M, Ghasemi-Fare O. Numerical investigation of various nanofluid heat transfers in microchannel under the effect of partial magnetic field: lattice Boltzmann approach. J Therm Anal Calorim. 2020;140:773–87. https://doi.org/10.1007/s10973-019-08862-w.
3. Karimipour A, Hossein-Nezhad A, D'Orazio A, Hemmat-Esfe M, Safaei R, Shirani E. Simulation of copper–water nanofluid in

a microchannel in slip flow regime using the lattice Boltzmann method. Eur J Mech B/Fluids. 2015;49(A):89–99. https://doi.org/10.1016/j.euromechflu.2014.08.004.
4. D'Orazio A, Karimipour A. A useful case study to develop lattice Boltzmann method performance: gravity effects on slip velocity and temperature profiles of an air flow inside a microchannel under a constant heat flux boundary condition. Int J Heat Mass Transf. 2019;136:1017–29. https://doi.org/10.1016/j.ijheatmasstransfer.2019.03.029.
5. Alipour P, Toghraie D, Karimipour A, Hajian M. Modeling different structures in perturbed Poiseuille flow in a nanochannel by using of molecular dynamics simulation: study the equilibrium. Phys A. 2019;515:13–30. https://doi.org/10.1016/j.physa.2018.09.177.
6. Alipour Lalami A, Hassanzadeh Afrouzi H, Moshfegh A. Investigation of MHD effect on nanofluid heat transfer in microchannels. J Therm Anal Calorim. 2019;136:1959–75. https://doi.org/10.1007/s10973-018-7851-1.
7. Hantao L, Yuxiang L, Shan J, Jianzhong C, Haijin H. Energy-conserving dissipative particle dynamics simulation of macromolecular solution flow in micro-channel under thermal convection. Eng Anal Boundary Elem. 2019;102:21–8. https://doi.org/10.1016/j.enganabound.2019.02.006.
8. Jafari S, Zakeri R, Darbandi M. DPD simulation of non-Newtonian electroosmotic fluid flow in nanochannel. Mol Simul. 2018;44(17):1444–53. https://doi.org/10.1080/08927022.2018.1517414.
9. Zarei A, Karimipour A, Meghdadi Isfahani A, Tian Z. Improve the performance of lattice Boltzmann method for a porous nanoscale transient flow by provide a new modified relaxation time equation. Phys A. 2019;535:122453. https://doi.org/10.1016/j.physa.2019.122453.
10. Javidi-Sarafan M, Alizadeh R, Fattahi A, Valizadeh-Ardalan M, Karimi N. Heat and mass transfer and thermodynamic analysis of power-law fluid flow in a porous microchannel. J Therm Anal Calorim. 2020. https://doi.org/10.1007/s10973-020-09679-8.
11. Ghani Dehkordi K, Karimipour A, Afrand M, Toghraie D, Meghdadi Isfahani AM. The electric field and microchannel type effects on H2O/Fe3O4 nanofluid boiling process: molecular dynamics study. Int J Thermophys. 2020;41:132. https://doi.org/10.1007/s10765-020-02714-8.
12. Asgari A, Nguyen Q, Karimipour A, Bach Q, Hekmatifar M, Sabetvand R. Develop molecular dynamics method to simulate the flow and thermal domains of H2O/Cu nanofluid in a nanochannel affected by an external electric field. Int J Thermophys. 2020;41:126. https://doi.org/10.1007/s10765-020-02708-6.
13. Hoogerbrugge PJ, Koelman JMVA. Simulating microscopic hydrodynamic phenomena with dissipative particle dynamics. Europhys Lett. 1992;19:155–60. https://doi.org/10.1209/0295-5075/19/3/001.
14. Hoogerbrugge PJ, Koelman JMVA. Dynamic simulations of hard-sphere suspensions under steady shear. Europhys Lett. 1993;21:363.
15. Español P. Dissipative particle dynamics with energy conservation. Europhys Lett. 1997;40(6):631–6. https://doi.org/10.1209/epl/i1997-00515-8.
16. Español P, Warren P. Statistical-mechanics of dissipative particle dynamics. Europhys Lett. 1995;30(4):191–6.
17. Li Z, Drazer G. Hydrodynamic interactions in dissipative particle dynamics. Phys Fluids. 2008;20(10):103601. https://doi.org/10.1063/1.2980039.
18. Qiao R, He P. Mapping of dissipative particle dynamics in fluctuating hydrodynamics simulations. J Chem Phys. 2008;128(12):126101. https://doi.org/10.1063/1.2897991.
19. Bolintineanu DS, Grest GS, Lechman JB, Pierce F, Plimpton SJ, Schunk PR. Particle dynamics modeling methods for colloid suspensions. Comput Particle Mech. 2014;1(3):321–56. https://doi.org/10.1007/s40571-014-0007-6.
20. Mou-Bin L, Jian-Zhong C, & Han-Tao L. DPD simulation of multiphase flow at small scales. In 2010 The 2nd International Conference on Computer and Automation Engineering (ICCAE). IEEE. 2010. https://doi.org/10.1109/iccae.2010.5451423.
21. Liu M, Meakin P, Huang H. Dissipative particle dynamics simulation of multiphase fluid flow in microchannels and microchannel networks. Phys Fluids. 2007;19(3):33302. https://doi.org/10.1063/1.2717182.
22. Liu M, Meakin P, Huang H. Dissipative particle dynamics simulation of pore-scale multiphase fluid flow. Water Resour Res. 2007. https://doi.org/10.1029/2006wr004856.
23. Litvinov S, Xie Q, Hu X, Adams N, Ellero M. Simulation of individual polymer chains and polymer solutions with smoothed dissipative particle dynamics. Fluids. 2016;1(1):7. https://doi.org/10.3390/fluids1010007.
24. Yang K, Vishnyakov A, Neimark AV. Polymer translocation through a nanopore: DPD study. J Phys Chem B. 2013;117(13):3648–58. https://doi.org/10.1021/jp3104672.
25. Jehser M, Zifferer G, Likos C. Scaling and Interactions of Linear and Ring Polymer Brushes via DPD Simulations. Polymers. 2019;11(3):541. https://doi.org/10.3390/polym11030541.
26. Kacar G. Dissipative particle dynamics simulation parameters and interactions of a hydrogel. J Turk Chem Soc Sect A Chem. 2017;10:1–12. https://doi.org/10.18596/jotcsa.309646.
27. Pan D, Phan-Thien N, Khoo BC. Dissipative particle dynamics simulation of droplet suspension in shear flow at low Capillary number. J Nonnewton Fluid Mech. 2014;212:63–72. https://doi.org/10.1016/j.jnnfm.2014.08.011.
28. Pan D, Phan-Thien N, Khoo BC. Studies on liquid–liquid interfacial tension with standard dissipative particle dynamics method. Mol Simul. 2014;41(14):1166–76. https://doi.org/10.1080/08927022.2014.952636.
29. Zhang Y, Xu J, He X. Effect of surfactants on the deformation of single droplet in shear flow studied by dissipative particle dynamics. Mol Phys. 2018;116(14):1851–61. https://doi.org/10.1080/00268976.2018.1459916.
30. Basan M, Prost J, Joanny JF, Elgeti J. Dissipative particle dynamics simulations for biological tissues: rheology and competition. Phys Biol. 2011;8(2):26014. https://doi.org/10.1088/1478-3975/8/2/026014.
31. Ye T, Phan-Thien N, Khoo BC, Lim CT. Dissipative particle dynamics simulations of deformation and aggregation of healthy and diseased red blood cells in a tube flow. Phys Fluids. 2014;26(11):111902. https://doi.org/10.1063/1.4900952.
32. Phan-Thien N, Mai-Duy N, Nguyen TYN. A note on dissipative particle dynamics (DPD) modelling of simple fluids. Comput Fluids. 2018;176:97–108. https://doi.org/10.1016/j.compfluid.2018.08.030.
33. Mai-Duy N, Phan-Thien N, Tran-Cong T. An improved dissipative particle dynamics scheme. Appl Math Model. 2017;46:602–17. https://doi.org/10.1016/j.apm.2017.01.086.
34. Abu-Nada E. Dissipative particle dynamics investigation of heat transfer mechanisms in Al_2O_3-water nanofluid. Int J Therm Sci. 2018;123:58–72. https://doi.org/10.1016/j.ijthermalsci.2017.09.005.
35. Abu-Nada E, Pop I, Mahian O. A dissipative particle dynamics two-component nanofluid heat transfer model: application to natural convection. Int J Heat Mass Transf. 2019;133:1086–98. https://doi.org/10.1016/j.ijheatmasstransfer.2018.12.151.
36. Abu-Nada E. Simulation of heat transfer enhancement in nanofluids using dissipative particle dynamics. Int Com in Heat Mass Transf. 2017;85:1–11. https://doi.org/10.1016/j.icheatmasstransfer.2017.04.008.

37. Okonkwo EC, Wole-Osho I, Almanassra IW, Abdullatif YM, Al-Ansari T. An updated review of nanofluids in various heat transfer devices. J Therm Anal Calorim. 2020. https://doi.org/10.1007/s10973-020-09760-2.
38. Alshare A, Al-Kouz W, Alkhalidi A, Kiwan S, Chamkha A. Periodically fully developed nanofluid transport through a wavy module. J Therm Anal Calorim. 2020. https://doi.org/10.1007/s10973-020-09448-7.
39. Tong Z, Liu H, Liu Y, Li H, Jiang S, Chang J, Hu S, Li G, Hao H. A study on the dynamic behavior of macromolecular suspension fow in micro–channel under thermal gradient using energy-conserving dissipative particle dynamics simulation. Microfuidics and Nanofuidics. 2020;24:34. https://doi.org/10.1007/s10404-020-02338-2.
40. Yaghoubi S, Shirani E, Pishevar, AR. Improvement of Dissipative Particle Dynamics method by taking into account the particle size. Scientia Iranica. 2018. https://doi.org/10.24200/sci.2018.21042.
41. Yaghoubi S, Shirani E, Pishevar AR, Afshar Y. New modified weight function for the dissipative force in the DPD method to increase the Schmidt number. EPL (Europhysics Letters). 2015;110(2):24002. https://doi.org/10.1209/0295-5075/110/24002.
42. Ripoll M, Español P, Ernst MH. Dissipative particle dynamics with energy conservation: heat conduction. Int J Mod Phys. 1998;9(8):1329–38. https://doi.org/10.1142/S0129183198001205.
43. Qiao R, He P. Simulation of heat conduction in nanocomposite using energy conserving dissipative particle dynamics. Mol Simul. 2007;33:667–83. https://doi.org/10.1080/08927020701286511.
44. He P, Qiao R. Self-consistent fluctuating hydrodynamics simulation of thermal transport in nanoparticle suspensions. J Appl Physiol. 2008;103(9):094305. https://doi.org/10.1063/1.2908217.
45. Borhani M, Yaghoubi S. Numerical simulation of heat transfer in a parallel plate channel and promote dissipative particle dynamics method using different weight functions. Int Com in Heat and Mass Transf. 2020;115:104606. https://doi.org/10.1016/j.icheatmasstransfer.2020.104606.
46. Abu-Nada E. Modeling of various heat transfer problems using dissipative particle dynamics. Numer Heat Transfer, Part A. 2010;58:660–7. https://doi.org/10.1080/10407782.2010.516681.
47. Abu-Nada E. Heat transfer simulation using energy conservative dissipative particle dynamics. Mol Simul. 2010;36(5):382–90. https://doi.org/10.1080/08927020903515337.
48. Mackie AD, Bonet D, Avalos JB, Navas V. Dissipative particle dynamics with energy conservation: modeling of heat flow. Phys Chem Chem Phys. 1999;1:2039–49. https://doi.org/10.1039/A809502G.
49. Yamada T, Kumar A, Asako Y, Gregory OJ, Faghri M. Forced convection heat transfer simulation using dissipative particle dynamics. Numer. Heat Transfer A. 2011;60(8):651–65. https://doi.org/10.1080/10407782.2011.616847.
50. Groot RD, Warren PB. Dissipative particle dynamics: bridging the gap between atomistic and mesoscopic simulation. J Chem Phys. 1997;107:4423–35. https://doi.org/10.1063/1.474784.
51. Cao ZH, Luo K, Yi HL, Tan HP. Energy conservative dissipative particle dynamics simulation of mixed convection in eccentric annulus. Int J Heat Mass Transf. 2014;74:60–76. https://doi.org/10.1016/j.ijheatmasstransfer.2014.03.022.
52. Abu-Nada E. Mixed convection simulation using dissipative particle dynamics. Numer Heat Transfer, Part A. 2015;67:808–25. https://doi.org/10.1080/10407782.2014.949178.
53. Tiwari A. Dissipative Particle Dynamics model for two phase flows, Ph.D.thesis, Purdue University, Purdue, 2006.
54. Xie Y, Chen S. Numerical simulation of heat transfer in microchannel using energy conservative dissipative particle dynamics. Adv Mech Eng. 2015;7(3):168781401557123. https://doi.org/10.1177/1687814015571230.
55. Laradji M, Kumar PBS. Dynamics of domain growth in self assembled fluid vesicles. Phys Rev Lett. 2004;93(19):198105. https://doi.org/10.1103/PhysRevLett.93.198105.
56. Yamada T, Hamian S, Sundén B, Park K, Faghri M. Diffusive-ballistic heat transport in thin films using energy conserving dissipative particle dynamics. Int J Heat Mass Transfer. 2013;61:287–92. https://doi.org/10.1016/j.ijheatmasstransfer.2013.02.011.